PHILOSOPHICAL TRANSACTIONS A

Phil. Trans. R. Soc. A.
doi:10.1098/not yet assigned

Advanced schemes for underdense plasma photocathode wakefield accelerators: Pathways towards ultrahigh brightness electron beams

GG Manahan[1,2,*], AF Habib[1,2], P Scherkl[1,2], D Ullmann[1,2], A Beaton[1,2], A Sutherland[1,2], G Kirwan[1,2,3], P Delinikolas[1,2], T Heinemann[1,2,3], R. Altuijri[1,2,4], A Knetsch[3], O Karger[5], N Cook[6], DL Bruhwiler[6], Z-M Sheng[1,2,7], JB Rosenzweig[8] and B Hidding[1,2]

[1]Scottish Universities Physics Alliance, Department of Physics, University of Strathclyde Glasgow G4 0NG, UK. [2]Cockcroft Institute, Sci-Tech Daresbury, Keckwick Lane, Daresbury, Cheshire WA4 4AD, UK. [3]Deutsches Elektronen-Synchrotron DESY, Hamburg, Germany. [4]Physics Department, Princess Nora Bint Abd Ulrahman University, Riyadh, Kingdom of Saudi Arabia. [5]Department of Experimental Physics, University of Hamburg, Hamburg, Germany. [6]RadiaSoft LLC, Boulder, Colorado, USA. [7]Laboratory for Laser Plasmas and School of Physics and Astronomy, Shanghai Jiao Tong University, China. [8]Particle Beam Physics Laboratory, University of California, Los Angeles, California, USA

Keywords: plasma wakefield acceleration, under-dense plasma photocathode, simultaneous spatial and temporal focusing, energy spread compensation

Summary

The "Trojan Horse" underdense plasma photocathode scheme applied to electron-beam driven plasma wakefield acceleration has opened up a path which promises high controllability and tunability and to reach extremely good quality as regards emittance and 5D beam brightness. This combination has the potential to improve the state-of-the-art in accelerator technology significantly. In this paper, we review the basic concepts of the Trojan Horse scheme and presents advanced methods for tailoring both the injector laser pulses and the witness electron bunches and combine them with the Trojan Horse scheme. These new approaches will further enhance the beam qualities, such as transverse emittance and longitudinal energy spread, and may allow, for the first time, to produce ultrahigh 6D brightness electron bunches, which is a necessary requirement for driving advanced radiation sources.

1. Introduction

Recently, plasma-based wakefield accelerators, driven by either highly intense laser pulse [1- 2] or relativistic electron beams [3-4], are globally seen as the next generation drivers for advanced radiation sources. Their potential applications for high energy physics are also recognised. This novel acceleration technique can harness high energy gains in laboratory scale (GV m^{-1}) because the generated plasma waves are capable of sustaining electric fields with amplitudes greater than E_0, the non-relativistic wave breaking field. Mathematically, E_0 can be expressed as $E_0\,\{\mathrm{V\,m^{-1}}\} \approx 96\sqrt{n_0\{\mathrm{cm^{-3}}\}}$, where n_0 is the background electron density of the plasma [5]. For instance, plasma with density of $n_0 = 10^{18}$ cm^{-3} can yield accelerating fields of ~ 96 GV m^{-1} – these are orders of magnitude greater than the achievable in conventional RF linacs. Hence, it is possible to realise cost-efficient and medium-scale accelerators. Today, production of quasi-monoenergetic, GeV-scale electron bunches within few cm accelerating length is routinely demonstrated worldwide [2, 4].

*Author for correspondence (grace.manahan@strath.ac.uk).

In the case of electron beam-driven plasma acceleration (PWFA), electron bunches can be accelerated with high efficiency through the blowout regime, a scenario of highly nonlinear plasma excitation [6-7]. The bunch density, n_b, of the electron beam driver with a bi-Gaussian distribution is described as $n_b = N_b/[(2\pi)^{3/2}\sigma_z\sigma_r^2]$, where N_b is total number of electrons, and σ_z and σ_r are the electron driver's bunch length and radial size. In this highly nonlinear regime, the electron driver bunch density is greater than the n_0 ($n_b/n_0 \gg 1$), such that the plasma electrons are completely expelled, creating a nearly spherical ion cavity, known as the blowout. Furthermore, high efficient excitation of the blowout is obtained when σ_z is smaller than the plasma wave number, k_p [8]. Inside the blowout, strong transverse focusing forces and GVm^{-1} level longitudinal fields are attainable. Hence, various electron injection schemes into this regime have been conceived and studied.

The process of electron injection into the plasma wakes plays a key role because the important beam parameters (such as normalised transverse emittance ϵ_n, energy spread $\Delta W/W$, total charge Q and bunch duration σ_z) are largely defined by the initial acceleration stage. The various electron bunch injections can be categorised into two: (i) via external injection [3-4] where an electron bunch with an initial energy and beam parameters are injected and further accelerated into a plasma blowout and (ii) via internal injection where the electrons accelerated are initially at rest and the residual transverse momentum is minimal. Example of these internal injection schemes are using plasma density transition [9-12] and those where additional electrons are release within trapping regions based on higher-level ionisation due to electron field or wakefield spikes [13-17]. One scheme, known as the underdense plasma photocathode (popularised as the Trojan Horse scheme) is based on ionisation injection triggered by a laser pulse. This scheme combines the long acceleration distances of electron-beam driven plasma wakes and limited peak electric fields of particle drivers with the controllability and tuneability of the laser pulses to release electrons directly inside the blowout [18-19]. In this method, electron bunches with transverse emittance as low as nm-rad is possible. Therefore, accelerators based on Trojan Horse scheme may lead to further step-change by increasing the tuneability and electron beam quality in terms of emittance and 5D brightness by orders of magnitude, where the B_{5D} is mathematically expressed as $B_{5D} = 2I_p/\epsilon_n^2$, where I_p is the peak current ($I_p = cQ/\sqrt{2\pi}\sigma_z$). Interestingly, the concept of laser-triggered ionisation has also been reported for application in laser wakefield acceleration, which can be found in these References [20-22] and have shown production of high quality electron beams.

In this article, we present an overview of the Trojan Horse scheme, its advantages, challenges and potential applications using the electron bunch generation. We also presents advanced and novel methods, which in combination with the Trojan Horse concept, aim to enhance the electron beam qualities and in consequence, will further boost the overall beam brightness.

2. Trojan Horse scheme: the underdense plasma photocathode wakefield acceleration

The Trojan Horse (TH) underdense plasma photocathode scheme requires underdense mixtures of low ionisation threshold (LIT) and high-ionisation threshold (HIT) species, such as Hydrogen and Helium (H/He). The high amplitude blowout based on the LIT component is driven by an electron beam, as in the conventional PWFA. Hydrogen, which have ionisation thresholds of $\xi_{i,H} = 13.6$ eV for atomic and $\xi_{i,H_2} = 15.4$ eV for molecular (H_2), is an ideal plasma source because it can be easily ionised either by a modest energy laser pulse or by the self-field of the electron beam driver.

The free electrons are released from the HIT component by a strongly focused, ultra-short laser pulse, which can be called as the TH injector laser. Helium is popularly used as HIT component because of its relatively high ionisation threshold ($\xi_{i,He} = 24.6$ eV). The peak amplitude of the normalised vector potential for the laser pulse used to ionise the HIT component can be as low as $a_0 \sim 0.01$. For a linearly polarised Gaussian beam, a_o is related to the laser peak intensity, I_L, as $a_0 \approx 0.85 \times 10^{-9}\, \lambda\,\{\mu m\}\sqrt{I_L\,\{W\,cm^{-2}\}}$, where λ is the laser central wavelength. Here, the laser pulse intensity can be as low as $I_L\{W\,cm^{-2}\} = 10^{15}/\lambda^2\{\mu m\}$ [5]. At these intensities, the oscillating electric fields are sufficient to induced tunnelling ionisation [23]. The injected electrons are then rapidly accelerated in the blowout. Because the HIT electrons can be selectively released at any point in the blowout (e.g. at the centre of the blowout, approximately the location of the minimum trapping potential [24]), thus the trapping requirements are substantially decreased.

Since the wakefield generation and electron bunch injection are completely decoupled in TH scheme, the electron beam production offers more tuneability. For instance, multibunches with high beam quality and controlled energies are obtainable with this method. By using synchronised TH injector lasers that are independently tuned, such as varying the

delays and having different foci, electrons are released at different positions inside the plasma blowout, and therefore with different energies [25].

One of the issues in PWFA, particularly in triggered ionisation injection schemes is the occurrence of dark current. Dark current is the result of uncontrollable self-injection of electrons ionised by electric field spikes or "hot-spots". These hot spots can be generated by either the (i) wake vertex due to the recombining plasma electrons and/or (ii) by the electron beam driver itself. Detailed studies for the optimisation of the electron and plasma dynamics have been carried through in Reference [26] and have obtained conditions for a dark-current free blowout suitable for the TH scheme. Using intensive 3D particle-in-cell simulations, it is found that to obtained a dark-current free scenario with TH scheme, a blowout radius must be at all times smaller than the fully pre-ionised plasma column width, otherwise the electrons near this blowout will overshoot and will not properly re-attracted; therefore the overall blowout dynamics collapses. These have been presented in details in Reference [26]. Recently, experimental breakthrough and signatures of the TH injection were obtained in the "E210: Trojan Horse PWFA" program of SLAC FACET-I [27].

In the following sections, we present methods of (i) tailoring the plasma photocathode laser to decrease the release volume of the HIT electrons, which might result in the reduction of the initial emittance of the electron bunches and (ii) modifying the accelerating fields of the blowout which can result in compensating the accumulated longitudinal energy spread and chirp of the injected electron bunches.

3. Simultaneous spatial and temporal focusing of plasma photocathode laser

In the TH scheme, the reduction in the transverse normalised emittance is a direct consequence of the extremely low residual transverse momentum, $p/m_e c \sim a_0/2$, from the underdense photocathode laser's ponderomotive force. Here, m_e is the electron mass and c is the speed of light. It is furthermore desirable to decrease the release volume of the HIT electrons to reduce both the initial phase space as well as the longitudinal phase mixing due to electrons being born off axis and at different betatron phases of the driving wake, [18, 28], which can both increase emittance.

One technique to reduce the longitudinal extension of the release region has been reported previously based on the collision of two ultra-short laser pulses in transverse geometry [20]. However, the collision of two lasers creates substantial experimental complexity and challenges in terms of alignment and timing. In this section, we propose the use of simultaneous spatial and temporal focusing (SSTF) of a single laser pulse, a technique known from material processing and microscopy [29-33], and study the applicability for the TH injector lasers. SSTF was first suggested in Ref. [34] for a related laser-driven two-pulse scheme. With SSTF combined with TH, it is capable of reducing the release length of the HIT electrons by more than an order of magnitude when compared with the Rayleigh length z_R of a pulse with the typical longitudinal Gaussian distribution.

In the SSTF method, a transverse spatial chirp of the pulse frequency components is generated before passing through a focusing element. This can be done, for example, by placing a single-pass grating pair (suggested by Ref. [35]) as sketched in Figure 1a, where the SSTF configuration is adapted for the TH accelerator. By carefully choosing the arrival time of the SSTF laser with respect to the electron beam driver, the axial peak intensity of the SSTF laser occurs at the centre of the blowout, indicated by the dashed ellipse in Figure1a.

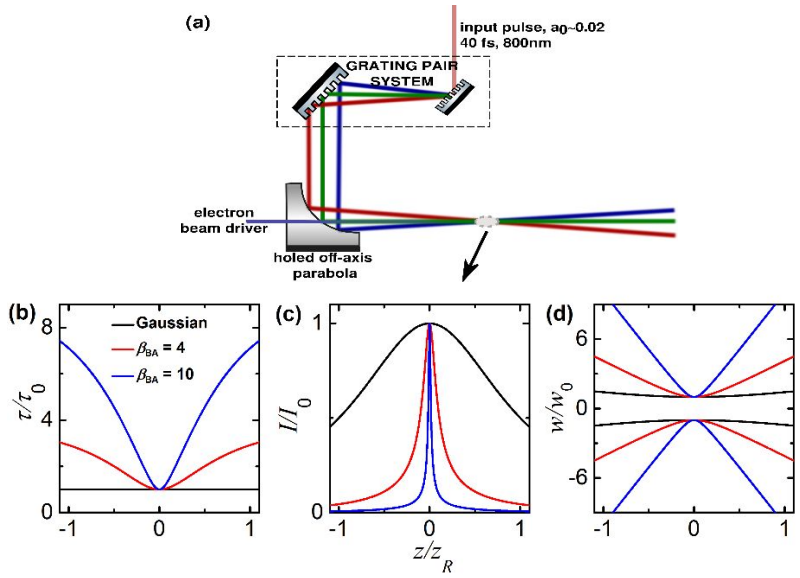

Figure 1: (a) Suggested set-up for the SSTF-TH scheme. A spatially chirped laser photocathode is focused at the location of the plasma blowout using an off-axis parabolic mirror. (b) Normalised pulse duration τ/τ_0, (c) the axial peak intensity I/I_0 and (d) transverse beam size w/w_0 of an SSTF pulse as a function of axial position z/z_R for different values of β_{BA}. The parameters are normalised to its corresponding non-spatially chirped pulse with axial Gaussian profile.

The following discussion of SSTF is mainly based on Ref. [35], where analytical study of SSTF is discussed. The spatially chirped laser can be considered analytically as a superposition of Gaussian beamlets, where each beamlet has a radius $(1/e^2)$ of w_{beamlet}, and is shifted from its central frequency ω_0. If the plasma photocathode laser has an initial spectral bandwidth of $\Delta\omega$, the position of each frequency component is $\alpha\,\Delta\omega$, where α is the chirp rate and can be expressed in dimensionless parameter as $\beta = \alpha\,\Delta\omega / w_{\text{beamlet}}$ [35]. At the entrance of the focusing element, the transverse profile is elongated along the axis where the chirp is applied due to the lateral stretching of the pulse. The amount of ellipticity can be characterized by a dimensionless parameter called beam aspect ratio, β_{BA}, which is defined as the beam radii $(1/e^2)$ ratio of the spatially chirped input pulses. It is expressed as: $\beta_{BA} = \sqrt{1+\beta^2}$ [35]. The frequency components recombine only at the focal region, where the smallest pulse duration is achieved (see Figure 1b). Away from the focus, the pulse is further stretched compared with an unchirped pulse, as shown in Figure 1b. An initial pulse with symmetric Gaussian distribution, $\lambda = 0.8$ µm, pulse length of $\tau_0 = 40$ fs, and a focus spot size of $w_0 = 4$ µm, is used for the calculation, giving a Rayleigh length of $z_R = 62$ µm. The structure of an SSTF pulse deviates from a typical Gaussian beam, in which the axial intensity strongly peaks at the focal position and drastically drops farther from the focus, as shown Figure 1c and Figure 2. For $\beta_{BA} = 4$, the FWHM of the axial intensity reduces to $z_{SSTF} \approx 13$ µm, more than 50% reduction compared to the z_R of the unchirped pulse. If the grating pair can produced spatial chirp with $\beta_{BA} = 14$, z_{SSTF} is further reduced down to 1 µm, more than an order of magnitude smaller than the z_R normally reached by conventional focusing.

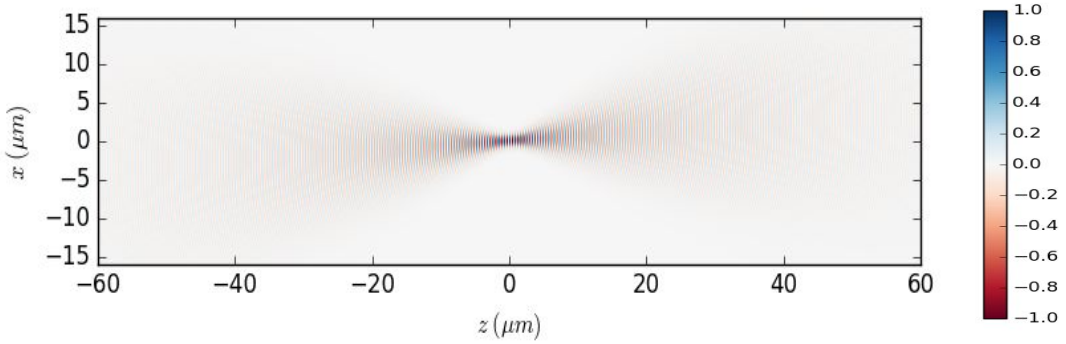

Figure 2: Field propagation of an SSTF pulse with beams aspect ratio of 4. Fields are normalised to 1.

It is important to note that the reduction on the FWHM of the axial intensity is primarily β_{BA} dependent, which can be changed by modifying the grating pair setup. On the other hand, the SSTF pulse maintains its transverse spot size, as

shown in Figure 1d. Here, it is shown that the beam diverges quickly with increasing β_{BA} value; this leads to lower intensities and longer pulse duration far from the focus. These analytical calculations show that with the SSTF method, the axial FWHM of the plasma photocathode laser can be compressed down to 1 μm without significantly changing the peak intensity and spot size. Figure 2 shows the field evolution of an SSTF pulse with beam aspect ratio of *4*, propagating in vacuum. Here, we can see that the fields are only at maximum within a small range of z near the focus location.

As an initial simulation, the SSTF-TH scheme is approximated with VSIM [36] particle-in-cell (PIC) simulations by artificially confining the HIT component in a very narrow region. These are carried through in 3D, which is necessary to catch the physics of the bunch generation and trapping process adequately. Simulation of longer acceleration distance and parameter scans are also required, which makes full resolution of the laser pulse resource-prohibitive. Instead, here we rely on analytical estimations of the release region volumes, and model the photocathode laser represented using an envelope approximation, propagating collinear and trailing 50 μm behind the electron beam driver. The HIT electron release is triggered by the laser pulse via advanced tunneling ionization implementation and geometrically fully resolved in transverse direction, but in the axial direction the release is artificially confined to the corresponding SSTF length as discussed above and plotted in Figures 1 and 2. For example, for an SSTF-TH laser with $\beta_{BA} = 14$, $w_0 = 4$ μm and a_0 0.02, the release length is confined to ~1 μm longitudinal length. A mixture of hydrogen and helium is used as LIT/HIT underdense medium. The electron beam driver has the following characteristics: energy $W = 23$ GeV, total charge $Q = 1$ nC, normalized rms emittance $\varepsilon_n = 2.25$ μm, rms width $\sigma_r = 20$ μm and rms length $\sigma_z = 30$ μm, corresponding to a bunch density $n_b \approx 2 \times 10^{17}$ cm^{-3}. The hydrogen component is preionized at a density of $n_H = 5 \times 10^{16}$ cm^{-3}, corresponding to a plasma wavelength $\lambda_p = \sqrt{\pi/n_H r_e} \approx 150$ μm, where r_e is the classical radius of an electron, while the He density is maintained to $n_H = 5 \times 10^{17}$ cm^{-3}.

Figures 3(a) and (b) show the wake driven by the electron beam immediately after when He electrons are (a) generated by a ~40 fs laser pulse inside the blowout at the focal region (equivalent to the longitudinal distance of $z = 400$ μm) and are (b) trapped and accelerated after 1 mm, where the bunch has gained a maximum energy of 10 MeV. In contrast to conventional TH, where the initial bunch distribution is rather cigar-like, since $z_R > w_0$, in SSTF-TH the initial bunch distribution is pancake-like, since $z_{SSTF} < w_0$. This can be seen in Figure 3a. From the initial results, the rms transverse emittance of the witness bunch using this SSTF approximation produces lower rms transverse emittance by an order of magnitude, as compared with the usual TH pulse that has Gaussian distribution. Note that the artificial confinement of the SSTF in these simulations is implemented because SSTF is a spatial chirp and thus the bandwidth of the laser pulse changes through propagation axis. Since we are using an envelope approximation in VSIM, the effect of the bandwidth on the dispersion of each frequency components of the laser in the plasma is not implemented. The consideration of the SSTF pulse dispersion in plasma is currently on going and will be discussed elsewhere.

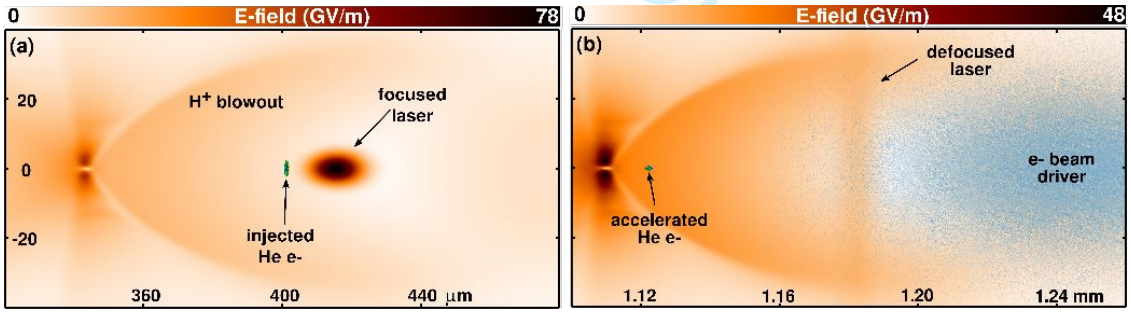

Figure 3: Snapshots from 3D PIC simulation immediately after (a) He generation and (b) after ~ 1 mm of acceleration.

4. Compact, plasma-based energy compensation technique

The high-energy acceleration in plasma inherently produces electron bunches with substantial longitudinal energy spread or chirp. This is well-known and is, currently, the central challenge in any plasma-based accelerators. The large energy spread is detrimental in several ways. Beam extraction and transport is difficult and leads to deterioration of the transverse emittance. It also limits the applications of these beams for advanced radiation sources. Therefore, the "energy spread and chirp problem" degrades the overall beam brightness and is a showstopper for fully harnessing the potentials of plasma-based accelerators.

Conventionally, 6D beam brightness is a figure of merit for comparing the quality of the radiation sources. High 6D brightness beams are characterised by high peak current, low transverse normalised emittance and narrow longitudinal energy spread. It is essential in many applications, such as to reach high-gain and shorter wavelengths in free-electron lasers [37] and for high-energy colliders, to enhance the focusability of the beam and increase its luminosity [38]. The 6D beam brightness can be expressed mathematically as $B_{6D} = B_{5D} \,/\, 0.1\%\, \Delta W_{\mathrm{rms}}/W \,\{\mathrm{Am}^{-1}/0.1\ \mathrm{BW}\}$.

In this section, a flexible scheme of tailoring the energy distribution of low-emittance electron beams inside a plasma-based accelerator is discussed, a concept which is initially introduced in Ref [39]. The tailoring process is based on beam-loading mechanism and can be tuned to achieve energy spread reduction without altering the electron beam emittance. In this concept, two moderate TH laser pulses are used to inject electrons to accelerating plasma wake and modify the field so that the accelerated low emittance electron beam of interest (called the witness bunch) will experience a longitudinal phase space rotation. This idea is one of the applications of the electron multibunch production as mentioned in Section 2. The loaded field reverses the effective accelerating gradient, and counter-rotates the accumulated longitudinal energy spread of the witness bunch. As a result, the energy spread is reduced, enabling the production of ultrahigh 6D brightness beams.

In this concept of plasma dechirper, the first TH laser releases the witness bunch at the beginning of the plasma stage. The parameters of the first TH laser is still the typical one used in any TH scheme, ie, $a_0 \ll 1$ and and strongly focus, e.g. spot size $w_0 < 5\ \mu\mathrm{m}$. This ensures that the injected electrons will obtained good beam qualities. After a period of acceleration, in which the witness bunch has gained sufficient energy and is stabilised, a second TH laser is introduced and this laser releases a second batch of electrons, which is called in Ref. [39] as the "escort bunch." The parameters (a_0, w_o and τ_0) of the second TH laser pulse are considerably higher than the first TH laser, such that the produced escort bunch will have a bunch charge density that is capable of overloading the wakefield. In Ref. [39], the escort bunch has gained a total charge of 100 pC in comparison to the witness bunch that is only 5 pC, and has shown that it significantly alters the longitudinal electric field. That means that the presence of the escort bunch strongly overloads the electric field. This results in the counter-clockwise rotation of the longitudinal phase space of the witness bunch while further accelerating. Consequently, the correlated energy spread is reduced reaching its minimum value, a position where extraction is ideal. The resulting energy compensation is shown in Figure 4, in which the phase space of the witness bunch at the position of the minimum energy spread is plotted. The extent of the overloaded field, known as the "dechirping region," must be much longer than the witness bunch such that the dechirping occurs from head to tail of the bunch. That means that the optimisation of the escort bunch must be focused on obtaining high charge and longer bunch duration than the witness bunch.

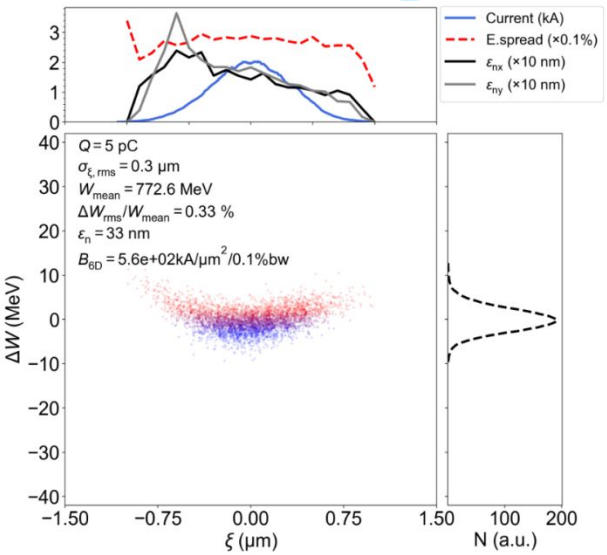

Figure 4: Longitudinal phase-space of the witness bunch during at the position of minimum energy spread from Ref [39].

The main challenges of this approach are the additional laser pulse to produce the escort bunch and the tuneability and spatiotemporal alignment accuracy of both laser pulses. To test how the alignment of the two TH laser pulses affect the plasma dechirping process, an initial jitter study is performed. For this initial analysis, the first TH laser is introduced with a transverse offset with respect to the blowout axis. The result is shown in Figure 5, where the dechirping distance, Δz, and the resulting uncorrelated energy spread is monitored. In this study, a comparable shorter plasma wavelength (λ_p

~ 100 μm) is used, corresponding to a blowout radius, $R_{b,max}$ is 40 μm. As shown in the plot, the dechirping distance and residual energy spread of the witness bunch is quite resilient to the jitter of the initial position of the first TH laser pulse, ie. the y-offset must be greater than $0.2*R_{b,max}$ to see a significant increase in the uncorrelated energy spread. Fortunately, the tolerance against spatiotemporal alignment jitters increases when considering longer plasma wavelengths (hence smaller plasma densities). This is because the plasma blowout increases both in longitudinal and transverse direction. The laser-to-electron drive beam jitter, however, is independent of the plasma wavelength, which means that at lower plasma densities it is easier to release the electrons consistently in the desired phase and at the right trapping position. Furthermore, the residual uncorrelated energy spread decreases when going to longer plasma wavelengths.

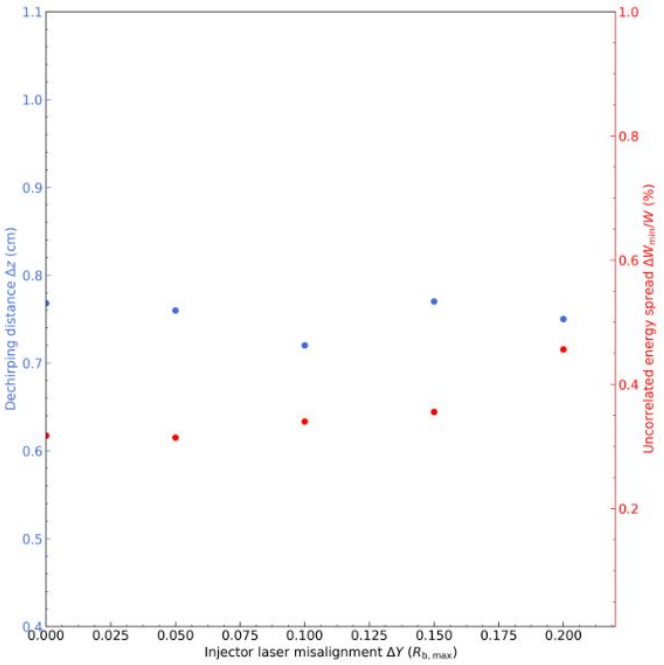

Figure 5: Effect of the first TH laser pulse offset to the plasma-based dechirping techniques. The initial position of TH laser is offset transversely with respect to the blowout axis. Here, the plasma wavelength is 100 μm, thereby the maximum blowout radius, $R_{b,max}$ is 40 μm.

5. Conclusions

In this paper, the Trojan Horse scheme is reviewed for the application in electron-beam driven plasma wakefield accelerator. The decoupling of the plasma blowout generation and electron injection allows greater tuneability and control of the acceleration process and witness bunch qualities, such as transverse emittance and 5D brightness. These developments in electron beam emittance and 5D-brightness may have transformative impact on key applications such as compact yet high performance free-electron lasers. Two advanced methods were presented and were proposed to integrate with the TH scheme. These combinations have the potential of further improving the witness bunch qualities and may pave the way of boosting the 6D beam brightness of the electron bunches.

Additional Information

Acknowledgement

We acknowledge the in-depth discussion of SSTF application to TH scheme with R. Lehe and S. Cook.

Funding Statement

This work used computational resources of the National Energy Research Scientific Computing Center, which is supported by DOE DE-AC02-05CH11231, and of JURECA (project hhh36), of HLRN, and Shaheen (project k1191), and the DFG Emmy-Noether program. This work was supported by a fellowship within the FIT worldwide programme of the

German Academic Exchange Service (DAAD), and by RadiaBeam Technologies. DLB would like to acknowledge DOE Office of Science award # DE-SC0013855.

Data Accessibility

Data are available upon request through the corresponding author.

Competing Interests

We have no competing interest.

Authors' Contributions

All authors contributed equally in this manuscript.

References

1. Wang X. et al. 2013. Quasi-monoenergetic laser-plasma acceleration of electrons to 2 GeV. *Nat. Commun*. **4**, 1988. (doi: 10.1038/ncomms2988)
2. Leemans WP. et al. 2014. Multi-GeV Electron Beams from Capillary-Discharge-Guided Subpetawatt Laser Pulses in the Self-Trapping Regime. *Phys. Rev. Lett.* **113**, 245002. (doi: 10.1103/PhysRevLett.113.245002)
3. Blumenfeld I. et al. 2007. Energy doubling of 42 GeV electrons in a metre-scale plasma wakefield accelerator. *Nature*. **445**, 741-4. (doi: 10.1038/nature05538)
4. Litos M. et al. 2014. High-efficiency acceleration of an electron beam in a plasma wakefield accelerator. *Nature*. **515**, 92-95. (doi: 10.1038/nature13882)
5. Esarey E., Schroeder CB and Leemans W. 2009. Physics of laser-driven plasma-based electron accelerators. *Rev. Mod. Physics*. **81**, 1229. (doi: 10.1103/RevModPhys.81.1229)
6. Rosenzweig J.B. et al. 1991. Acceleration and focusing of electrons in two-dimensional nonlinear plasma wakefields. *Phys. Rev. A*. **44**, R6189-R692. (doi: 10.1103/PhysRevA.44.R6189)
7. Lu W. et al. 2006. Nonlinear theory for relativistic plasam wakefields in the blowout regime. *Phys. Rev. Lett*. **96**, 165002. (doi: 10.1103/PhysRevLett.96.165002)
8. Barov N., Rosenzweig JB., Thompson MC., and Yoder RB. 2004. Energy loss of a high-charge bunched electron beam in plasma: Analysis. *Phys. Rev. Accel. Beams*. 7, 061301. (doi: 10.1103/PhysRevSTAB.7.061301)
9. Suk H., Barov N., Rosenzweig JB. and Esarey E. 2001. Plasma Electron Trapping and Acceleration in a Plasma Wake Field Using a Density Transition. *Phys. Rev. Lett*. **86**, 1011-1014. (doi: 0.1103/PhysRevLett.86.1011)
10. Geddes CGR. et al. Plasma-density gradient injection of low absolute momentum spread electron bunches. *Phys. Rev. Lett.* **100**, 215004. (doi: 10.1103/PhysRevLett.100.215004)
11. Bulanov S. et al. 1998.Particle injection into the wave acceleration phase due to nonlinear wave wake breaking. *Phys. Rev. E.* **58**, R5257-R5260. (doi:10.1103/PhysRevE.58.R5257)
12. Xu XL. et al. 2017. High quality electron bunch generation using a longitudinal density-tailored plasma-based accelerator in the three-dimensional blowout regime. *Phys. Rev. Accel. Beams.* **20**, 111303. (doi: 10.1103/PhysRevAccelBeams.20.111303)
13. Umstadter D., Kim JK. and Dodd E. 1995. Method and apparatus for generating and accelerating ultrashort pulses. US Patent Serial No. 5789876.
14. Chen M. et al. 2006. Electron injection and trapping in a laser wakefield by field ionization to high-charge states of gases. *Journ. Applied Phys.* **99**, 056109. (doi: 10.1063/1.2179194)
15. Oz E. et al. 2007. Ionization-induced electron trapping in ultrarelativistic plasma wakes. *Phys. Rev. Lett.* **98**, 084801. (doi: 10.1103/PhysRevLett.98.084801)
16. Pak A et al. 2010. Injection and trapping of tunnel-ionized electrons into laser-produced wakes. *Phys. Rev. Lett.* **104**, 025003. (doi: 10.1103/PhysRevLett.104.025003)
17. Martinez de la Ossa A. et al. 2013. High-quality electron beams from beam-driven plasma accelerators by wakefield-induced ionization injection. *Phys. Rev. Lett.* **111**, 245003. (doi: 10.1103/PhysRevLett.111.245003)
18. Hidding B. et al. 2012. Ultracold electron bunch generation via plasma photocathode emission and acceleration in a beam-driven plasma blowout. *Phys. Rev. Lett.* **108**, 035001. (doi:10.1103/PhysRevLett.108.035001)
19. Xi Y. et al. 2013. Hybrid modeling of relativistic underdense plasma photocathode injectors. *Phys. Rev. ST Accel. Beams.* **16**, 031303. (doi: 10.1103/PhysRevSTAB.16.031303)

20. Li F. et al. 2013. Generating high-brightness electron beams via ionization injection by transverse colliding lasers in plasma-wakefield accelerator. *Phys. Rev. Lett.* **111**, 015003. (doi: 10.1103/PhysRevLett.111.015003)
21. Yu LL. et al. 2014. Two-color laser ionization injection. *Phys. Rev. Lett.* **112**, 125001. (doi: 10.1103/PhysRevLett.112.125001)
22. Xu XL. et al. 2016. Nanoscale electron bunching in laser-triggered ionization injection in plasma accelerators. *Phys. Rev. Lett.* **117**, 034801. (doi:10.1103/PhysRevLett.117.034801)
23. Chen M. et al. 2013. Numerical modeling of laser tunnelling ionization in explicit particle-in-cell codes. *Journ. Comp. Phys.* **236**, 220-228. (doi:10.1016/j.jcp.2012.11.029)
24. Pak, A. et al. 2010. Injection and trapping of tunnel-ionized electrons into laser-produced wakes. *Phys. Rev. Lett.* **104**.025003. (doi: 10.1103/PhysRevLett.104.025003)
25. Hidding et al. 2014. Tunable electron multibunch production in plasma wakefield accelerators. arXiv:1403.1109
26. Manahan GG. et al. 2016. Hot spots and dark current in advanced plasma wakefield accelerators. *Phys. Rev. Accel. Beams.* **19**, 011303. (doi: 10.1103/PhysRevAccelBeams.19.011303)
27. Hidding B. et al. 2017. First measurements of Trojan Horse injection in a plasma wakefield accelerator. *Proc. Of IPAC 2017*. 1252-1257.
28. Xu, XL. et al. 2014. Phase-space dynamics of ionization injection in plasma-based accelerators. *Phys. Rev. Lett.* **112**, 035003. (doi: 10.1103/PhysRevLett.112.035003)
29. Oron D., Tal E. and Silberberg Y. 2005. Scanningless depth-resolved microscopy. *Opt. Exp.* **13**, 1468. (doi: 10.1364/OPEX.13.001468)
30. Durst ME., Zhu G. and Xu C. 2006. Simultaneous spatial and temporal focusing for axial scanning. *Opt. Exp.* **14**, 12243-12254 (doi: 10.1364/OE.14.012243)
31. Durst ME., Zhu G. and Xu C. 2007. Simultaneous spatial and temporal focusing in nonlinear microscopy. *Opt. Commun.* **281**, 1796-1805. (doi: 10.1016/j.optcom.2007.05.071)
32. Block E. et al. 2013. Simultaneous spatial and temporal focusing for tissue ablation. *Biomed. Opt. Exp.* **4**, 831-841. (doi: 10.1364/BOE.4.000831)
33. Kammel R. e al. 2014. Enhancing precision in fs-laser material processing by simultaneous spatial and temporal focusing. *Light: Science & Applications.* **3**, e169. (doi: 10.1038/lsa.2014.50)
34. Bourgeois N., Cowley J. and Hooker SM. 2013. Two-pulse ionization injection into quasilinear laser wakefields. *Phys. Rev. Lett.* **111**, 155004. (doi: 10.1103/PhysRevLett.111.155004)
35. Durfee CG. et al. 2012. Intuitive analysis of space-time focusing with double-ABCD calculation. *Opt. Exp.* **20**, 14244. (doi: 10.1364/OE.20.014244)
36. Nieter, C. and Cary, J.R. 2004. VORPAL: A versatile plasma simulation code. *J. Comp. Physics*. **196**. 448-478. (doi: 10.1016/j.jcp.2003.11.004)
37. Di Mitri S. 2015. On the importance of electron beam brightness in high gain free electron lasers. *Photonics*. **2**, 317-341. (doi: 10.3390/photonics2020317)
38. Emma P. and Raubenhemier T. 2001. Systematic approach to damping ring design. *Phys. Rev. Accel. Beams.* **4**, 021001. (doi: 0.1103/PhysRevSTAB.4.021001)
Manahan GG. et al. 2017. Single-stage plasma-based correlated energy spread compensation for ultrahigh 6D brightness electron beams. *Nat. Commun*. **8**, 15705. (doi: https://doi.org/10.1038/ncomms15705)

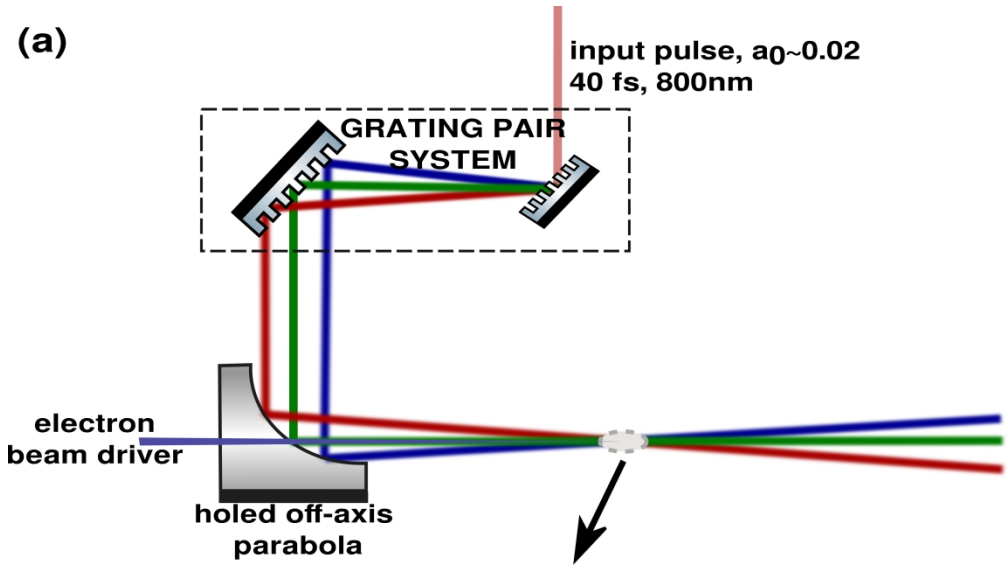

Figure 1: (a) Suggested set-up for the SSTF-TH scheme. A spatially chirped laser photocathode is focused at the location of the plasma blowout using an off-axis parabolic mirror.

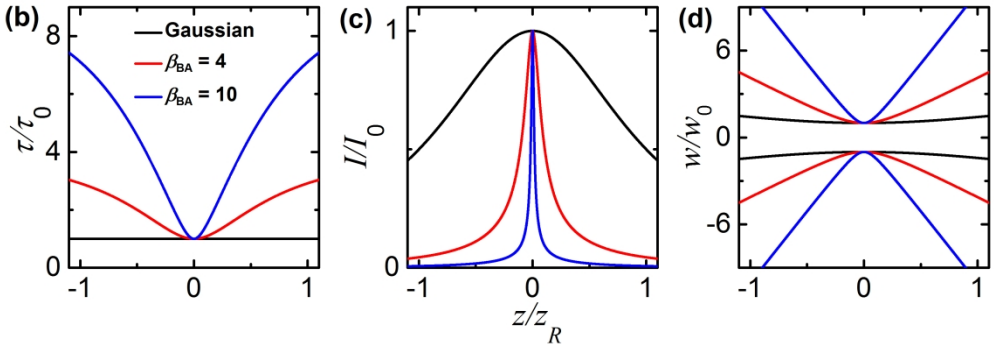

Figure 1 (b) Normalised pulse duration □/□0, (c) the axial peak intensity I/I0 and (d) transverse beam size w/w0 of an SSTF pulse as a function of axial position z/zR for different values of □BA. The parameters are normalised to its corresponding non-spatially chirped pulse with axial Gaussian profile.

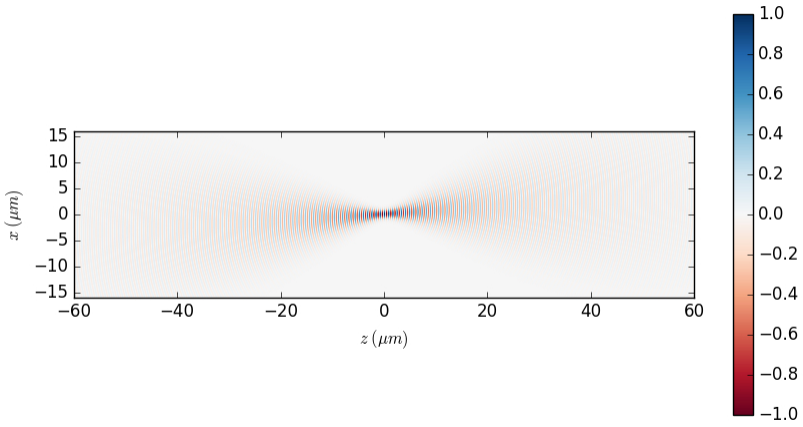

Figure 2: Field propagation of an SSTF pulse with beams aspect ratio of 4. Fields are normalised to 1.

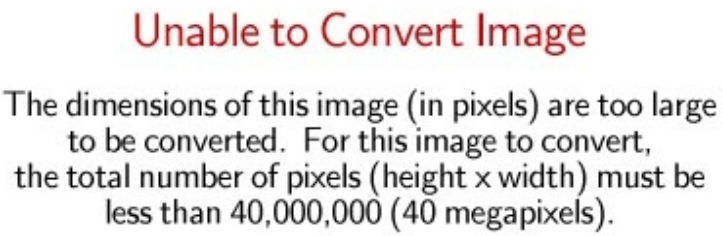

Figure 3: Snapshots from 3D PIC simulation immediately after (a) He generation and (b) after ~ 1 mm of acceleration.

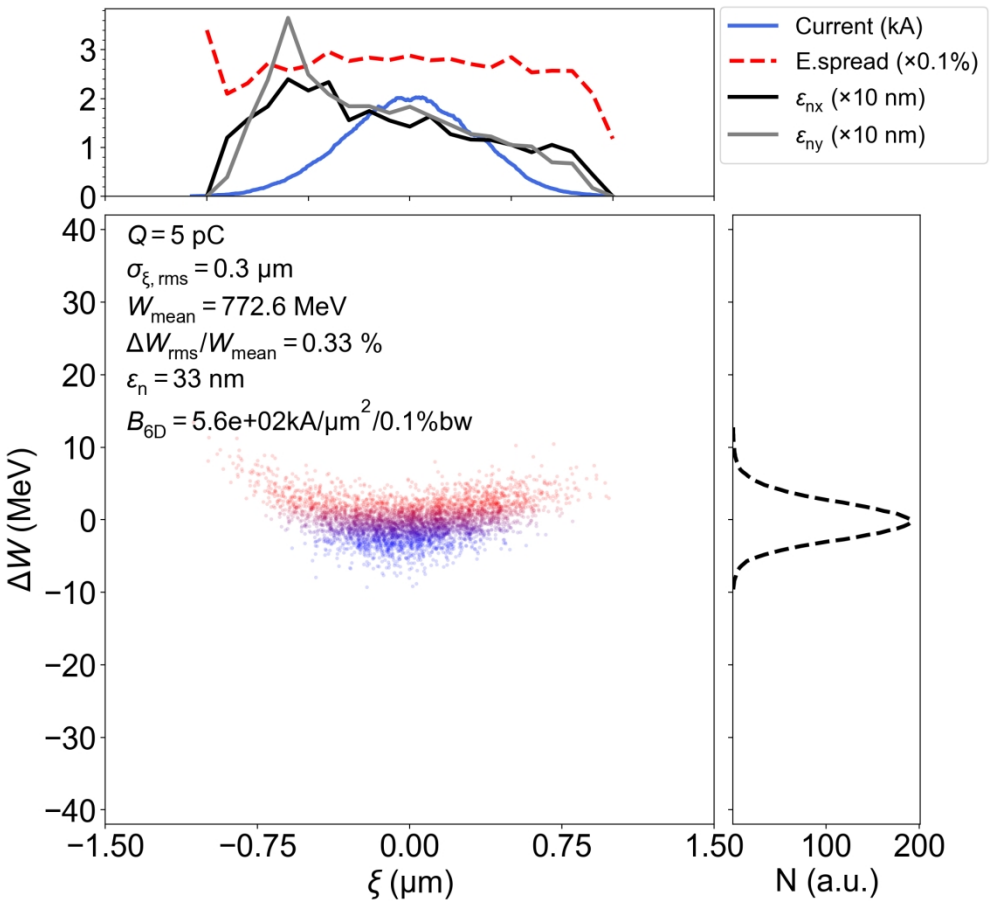

Figure 4: Longitudinal phase-space of the witness bunch during at the position of minimum energy spread from Ref [39].

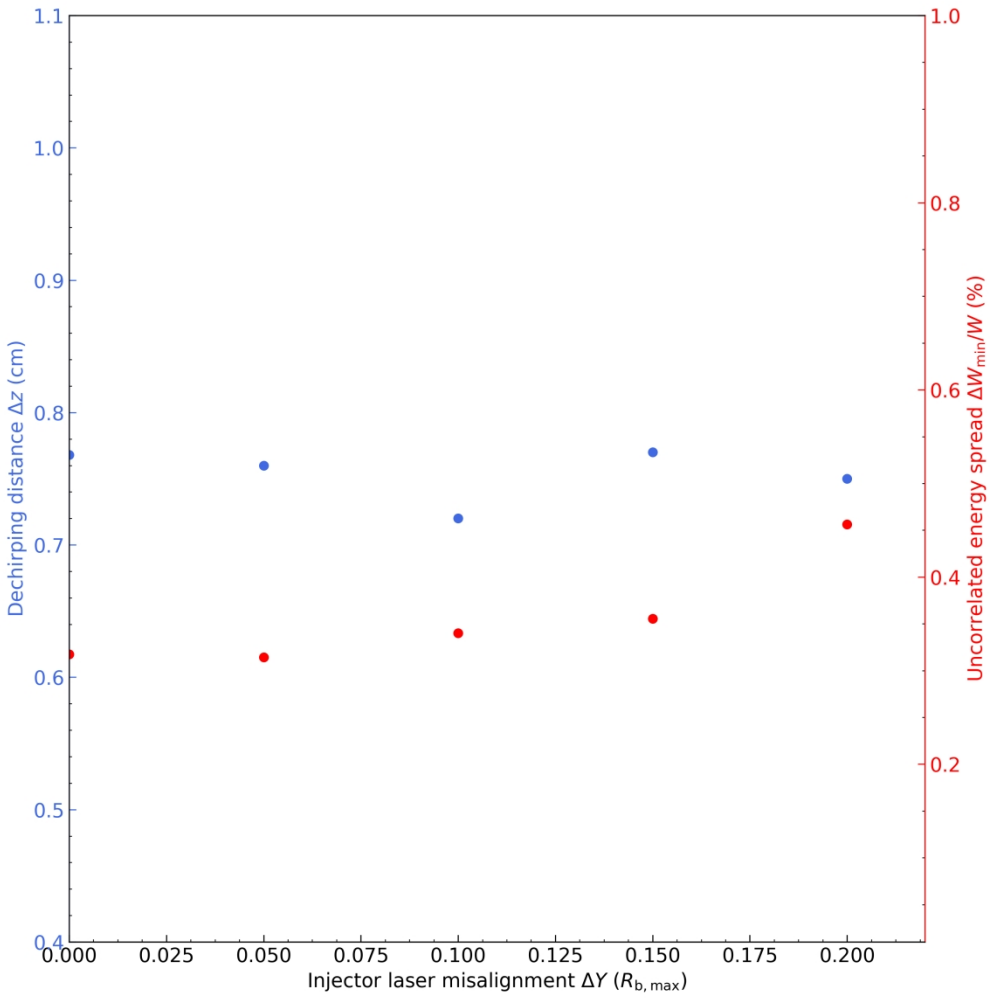

Effect of the first TH laser pulse offset to the plasma-based dechirping techniques. The initial position of TH laser is offset transversely with respect to the blowout axis. Here, the plasma wavelength is 100 μm, thereby the maximum blowout radius, Rb,max is 40 μm.